

GAME: Genetic Algorithms with Marginalised Ensembles for model-independent reconstruction of cosmological quantities

M. Peronaci,^{a,b,c} **M. Martinelli**,^{d,e} **S. Nesseris**,^f

^aDipartimento di Fisica, Università di Roma “Tor Vergata”, Via della Ricerca Scientifica 1, 00133, Roma, Italy

^bIstituto Nazionale di Fisica Nucleare (INFN), Sezione di Roma 2, Via della Ricerca Scientifica 1, 00133, Roma, Italy

^cDipartimento di Fisica, Università di Roma “Sapienza”, Piazzale Aldo Moro 5, 00185, Roma, Italy

^dINAF - Osservatorio Astronomico di Roma, via Frascati 33, 00078 Monte Porzio Catone, Italy

^eIstituto Nazionale di Fisica Nucleare (INFN), Sezione di Roma, P.le A. Moro 5, I-00185, Roma, Italy

^fInstituto de Física Teórica (IFT) UAM-CSIC, Calle Nicolás Cabrera 13-15, Campus de Cantoblanco UAM, 28049 Madrid, Spain

E-mail: matteo.peronaci@roma2.infn.it

Abstract. Genetic Algorithms (GA) are a powerful tool for stochastic optimisation and non-parametric symbolic regression, already widely used in cosmology. They are capable of reconstructing analytical functions directly from data points without introducing new physical models. A limitation of this approach is that while the reconstructed function is very efficient at reproducing the behaviour of the data points, non-observable quantities involving derivatives are particularly sensitive to stochasticity, hyperparameters, and to the choice of the best-fit function obtained by the GA, which implies the risk of the algorithm getting stuck in a local minimum. In this work we propose an update to the GA methodology for the reconstruction of analytical functions that involves computing a weighted average of an ensemble of GA configurations (GAME). We define the weights via a quantity that accounts for both the goodness-of-fit of the points and the smoothness of the resulting function. We also present a practical method to analytically estimate and correct the errors on the averaged function by combining a path-integral approach with an ensemble variance. We demonstrate the improvement offered by GAME methodology on a generic test function. We then apply the new methodology to a non-parametric reconstruction of the Hubble rate $H(z)$ using Cosmic Chronometers data and, assuming a flat Friedmann-Lemaître-Robertson-Walker background and General Relativity, we infer the corresponding dark energy equation of state $w(z)$. Through consistency tests, we show that current data produces results compatible with Λ CDM, and that Stage IV cosmology surveys will allow GA reinforced with GAME methodology to become an even more competitive tool for discriminating between different models.

Contents

1	Introduction	1
2	Genetic Algorithms methodology	3
2.1	Practical example	3
2.2	Standard GA reconstruction	4
2.2.1	χ^2 marginalisation	5
2.2.2	Error analysis: path-integral	6
2.3	Ensemble of hyperparameter models	8
2.3.1	Marginalisation over the ensemble (GAME)	9
2.3.2	Error analysis: ensembling and total uncertainty	12
2.3.3	Improvements in the reconstruction	13
3	Application to cosmological quantities	15
3.1	Dark energy equation of state	15
3.2	Testing Λ CDM with current data surveys	16
3.2.1	Reconstruction of $H(z)$	16
3.2.2	Derivation of $w(z)$	16
3.3	Forecasts with future data surveys	18
3.3.1	Reconstruction of $H(z)$	19
3.3.2	Derivation of $w(z)$	20
4	Conclusions and outlook	21
A	Testing ΛCDM with a subset of current data	25
A.1	Impact on the reconstruction of $H(z)$	25
A.2	Impact on the derivation of $w(z)$	26
B	Hyperparameter configurations setup	27

1 Introduction

The standard cosmological model, Λ CDM, has achieved unparalleled success in describing a wide range of observations [1], from the anisotropies of the Cosmic Microwave Background (CMB) to the large-scale distribution of galaxies. Within Einstein’s equations of General Relativity (GR), this success relies on the introduction of Cold Dark Matter (CDM) and dark energy in the form of a cosmological constant Λ . Despite its effectiveness, the model still faces major open questions: the unknown nature of the CDM component and of Λ , as well as prominent observational tensions in the measurements of the Hubble constant H_0 [2, 3]. While these issues suggest that Λ CDM might not be a complete description of the universe, there is currently no compelling alternative model that satisfactorily solves this tension [4]. Consequently, we might want to let data guide us towards the construction of new physical models.

This necessitates the search for robust model-independent and non-parametric reconstructions that can probe cosmological functions directly from data, minimising theoretical

priors and parametrisations. A particularly promising direction is to test the consistency between the cosmic expansion history and the properties of dark energy inferred from it. In GR, the background expansion and the physical content of the universe are tightly linked: if we reconstruct the expansion rate $H(z)$ and infer an effective dark energy equation of state $w(z)$, any significant and statistically robust deviation from $w(z) = -1$ could point to new physics. The difficulty lies in the fact that consistency tests based on non-observable quantities often require derivatives of reconstructed functions, making them especially sensitive to hyperparameters, overfitting, and the smoothness of the best-fit function.

Various non-parametric methods have been employed to address this, most notably Gaussian Processes (GP) [5, 6]. GP provides a fully bayesian reconstruction of a function and its derivatives, requiring the definition of a kernel function, which is in charge of controlling the correlations between different points of the reconstructed function [7]. However, although GP enable model-independent reconstructions by choosing a zero mean function to minimise cosmological assumptions, they can be sensitive to the choice of the kernel hyperparameters [8]. In this work, we focus on Genetic Algorithms (GA) [9, 10], a symbolic-regression technique capable of reconstructing analytical functions from data without introducing new physical parameters. Unlike GP, GA return explicit functional forms that can be more easily interpretable than kernel-based representations. However, a known limitation is that the GA best-fit function can reproduce the data extremely well, yet non-observable quantities involving derivatives can be fragile. Indeed, different GA runs (or different hyperparameter configurations) may generate similarly good fits that present noticeably different derivatives. This methodology has been successfully applied in various cosmological contexts, such as performing null tests of the cosmological constant model [11–13], for building emulators for complex observables [14–18], performing searches for new physics beyond Λ CDM [19–22], design quantum optics experiments and related quantum optimization algorithms [23, 24], etc.

We therefore propose an update to the standard GA¹ approach based on a model-averaging procedure over an ensemble of GA reconstructions. The key idea is to compute a weighted average of many GA best-fit functions in order to reduce the uncertainty due to stochasticity or to a particular choice of hyperparameters configuration, defining weights through a combined estimator that accounts not only for the goodness-of-fit (via χ^2) but also for smoothness (via a roughness penalty). We refer to this marginalised ensemble methodology as **GAME**² (Genetic Algorithms with Marginalised Ensembles).

In addition, since a model-averaged reconstruction requires a consistent uncertainty estimate, we introduce a practical method to estimate and combine both the measurement-driven statistical uncertainty, computed through a path-integral uncertainty approach [10], and an additional configuration-driven uncertainty quantified by the weighted variance across the ensemble. We validate the improvement on a generic test function $f(x)$ and then apply GAME to the reconstruction of the Hubble rate $H(z)$ using Cosmic Chronometers (CC) data. Finally, assuming a Friedmann-Lemaître-Robertson-Walker (FLRW) background and GR, we derive the corresponding dark energy equation of state $w(z)$ and compare it with the Λ CDM expectation. We also generate a set of mock data with the characteristics of Stage IV surveys in order to additionally validate and test GAME methodology's robustness.

This paper is structured as follows. In Section 2 we review the standard GA framework and present the GAME marginalisation methodology, then describe the corresponding total un-

¹<https://github.com/snessseris/Genetic-Algorithms>

²<https://github.com/matteoperonaci/GAME>

certainty estimation. In Section 3 we apply **GAME** to cosmological observables, reconstructing $H(z)$ from CC data and deriving the dark energy equation of state $w(z)$, and we then test performance on Stage IV-like mock datasets. We conclude in Section 4 with a summary of the results and possible extensions of the work.

2 Genetic Algorithms methodology

Genetic Algorithms (GA) are a model-independent machine learning tool for symbolic regression. They follow the principles of biological evolution via natural selection, where a population of mathematical functions, often referred to as chromosomes, evolves over time. In this context, a chromosome represents the analytical string of a function, and this evolution occurs under the influence of operations such as crossover (the combination of two different chromosomes to create an offspring) and mutation (a random change in one chromosome) [10].

The algorithm begins with an initial population of candidate individuals: N_{pop} functions randomly generated (analogous to traditional Monte Carlo approaches) based on a defined set of basic functions (\sin , \cos , \log , polynomial, \exp , etc.) and operators ($+$, $-$, \times , \div). Together, these elements constitute a set we refer to as the **grammar**. The algorithm is fed with N_{data} points in the form (x_i, y_i, σ_i) and establishes the adequacy of each function to represent the data points by calculating the χ^2 which, for uncorrelated measurements, is:

$$\chi^2 = \sum_{i=1}^{N_{\text{data}}} \left(\frac{f_j(x_i) - y_i}{\sigma_i} \right)^2, \quad \text{with } j = 1, \dots, N_{\text{pop}}, \quad (2.1)$$

where $f_j(x_i)$ is one of the N_{pop} functions generated by the GA. The χ^2 is then computed for each individual function in the population.

After generating the first population of functions, the algorithm starts producing the next generation by selecting a percentage of the best individuals (i.e., the functions with the minimum χ^2 values) from the previous population. Once selected, these optimal individuals are combined through crossover and mutation to produce offspring. After the new population is generated, the algorithm repeats until a termination goal is achieved, such as a minimum χ^2 value or a maximum number of generations N_{gen} . Finally, the best-fit analytical function returned at the end of the iteration is the one presenting the minimum χ^2 .

The grammar, number of individuals in the population, selection percentage, crossover and mutation probability, number of generations, and stochastic seed constitute the hyperparameters of the GA; they affect how fast the GA converges to the best-fit and the complexity of the final expression.

2.1 Practical example

We present a simplified example of a standard GA iteration to explain how it determines the best-fit function given a dataset of N_{data} . The following hyperparameters are fixed:

- $N_{\text{gen}} = 100$;
- $N_{\text{pop}} = 3$;
- **grammar** = polynomial, exponential, trigonometric;
- **selection rate** = 2/3;

- `crossover rate` = 0.8;
- `mutation rate` = 0.3;
- `random seed` = 12345;

The first population $\mathcal{F}(n_{\text{gen}} = 0)$ (with $n_{\text{gen}} = 0, \dots, N_{\text{gen}}$) of N_{pop} functions is generated randomly, according to the `random seed` and the `grammar`. Let us assume the initial N_{pop} functions are:

$$\mathcal{F}(0) = \{x^2, \exp x, \sin x\}. \quad (2.2)$$

Initially, the algorithm computes the χ^2 for each function in $\mathcal{F}(0)$ using the Equation (2.1) with the data points. Let us assume we obtain:

$$\vec{\chi}^2(0) = \{300, 200, 600\}. \quad (2.3)$$

The algorithm sorts the population with respect to χ^2 . Since the fixed `selection rate` is 2/3, it selects the two best functions out of the three. These are, respectively, the second ($\exp x$) and the first (x^2). Once the best functions are sorted and selected, the first generation begins, and the algorithm combines and modifies them via crossover and mutation, replacing all non-selected function slots (in this case, just the third remaining slot). One might obtain:

$$\mathcal{F}(1) = \left\{ \exp x, x^2, \frac{\exp x^3}{x^2} \right\}. \quad (2.4)$$

Once $\mathcal{F}(1)$ is generated, the algorithm computes $\vec{\chi}^2(1)$ and repeats the process. Finally, at the final generation (in our case $N_{\text{gen}} = 100$), we will have a population $\mathcal{F}(n_{\text{gen}} = 100)$ consisting of analytical and likely complex functions, alongside the final vector $\vec{\chi}^2(100)$. At this point, the analytical function associated with the minimum χ^2 is selected as the final output of the algorithm, referred to as $f_{\text{GA}}(x)$:

$$\chi_{\min}^2 = \min \vec{\chi}^2(100), \longrightarrow f_{\text{GA}}(x) = \mathcal{F}_{\chi_{\min}^2}(100). \quad (2.5)$$

Equation (2.5) can be read as the function coming out of the last generation that presents the minimum χ^2 , that is the function that better reproduce the input data points.

2.2 Standard GA reconstruction

To demonstrate the algorithm in action and illustrate the proposed improvement, we follow the procedure described in [10]. First, we generate a set of 20 sparse mock data points (x_i, y_i, σ_i) based on the model:

$$f(x; a, b, c) = a + (x - b) \cdot e^{-cx^2}, \quad (2.6)$$

where the parameters are $(a, b, c) = (0.75, 0.25, 0.10)$. The objective of GA is to generate a symbolic analytical function that reproduces the underlying $f(x)$ model only from data points.

We selected a function that exhibits smooth behaviour and possesses a maximum on purpose, to demonstrate that this methodology is capable of detecting the features underlying the function we are attempting to reconstruct. Then, to establish a benchmark for comparison, we minimised $\chi_i^2(a, b, c)$ from Equation (2.1) with respect to the parameters (a, b, c) .

We refer to the obtained result as $\chi^2_{\text{threshold}}$, representing the value obtained from a standard parametric analysis that we aim to surpass with a non-parametric algorithm. Next, we fix a set of hyperparameters for the GA and let the algorithm generate the best-fit function. Figure 1 shows the evolution of the χ^2 of the GA-generated function against the number of generations n_{gen} . Once the algorithm converges, if the curve goes below the threshold set by the standard parametric approach, it means we obtain an analytical function that fits data better than the one obtained from the model-dependent parameter minimisation.

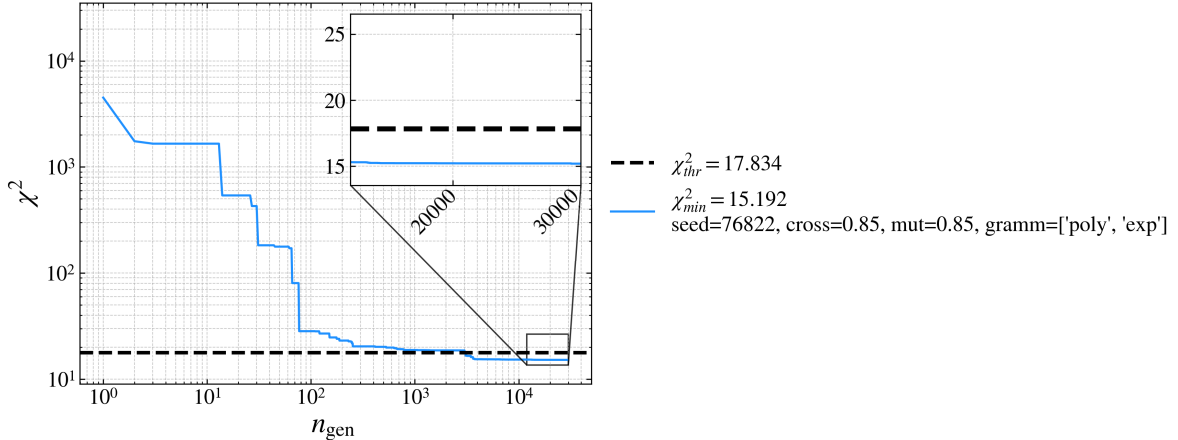


Figure 1. Evolution of the GA χ^2 with the number of generations n_{gen} . The black dotted line is the $\chi^2_{\text{threshold}}$, representing the χ^2 we aim to overcome, obtained through standard model-dependent minimisation of the parametrised function. The blue curve represents the χ^2 of the function generated by the GA. In the legend the hyperparameters setup of the GA are listed: the random seed is 76822, the probability of crossover and mutation is 85%, the grammar set for the generation is made of polynomial and exponential functions, the number of generations is $N_{\text{gen}} = 30000$, sufficient for χ^2_{GA} to drop below $\chi^2_{\text{threshold}}$.

2.2.1 χ^2 marginalisation

Given that GA rely entirely on the estimator used to establish whether a function adequately represents data (in our case, the χ^2), it is often useful to incorporate simple statistical techniques to refine the reconstruction process. A practical approach is to assume that the underlying model may differ from the GA reconstruction function by a constant y_0 . Depending on the problem, this constant can act as an additive offset (e.g. an uncertain zero-point) or as a multiplicative normalisation (e.g. an unknown overall scale).

- **Additive offset:** $y(x) = y_0 + f_{\text{GA}}(x)$;
- **Multiplicative offset:** $y(x) = y_0 \cdot f_{\text{GA}}(x)$.

Physically, the additive offset is helpful when dealing with a calibration or systematic error that may add a constant independent on the overall reconstructed function. On the other side, the multiplicative offset is suited when dealing with a normalisation factor of the quantity we are interested in reconstructing. For the Hubble rate, and analogously the test function, we are more interested in the shape of $H(z)$, while the overall normalisation is set by the Hubble constant H_0 , so it is natural to treat H_0 as a multiplicative offset.

We want to re-define the χ^2 to take into account eventual offsets ([25–28]). Inserting these expressions into the standard uncorrelated χ^2 in Equation (2.1), the χ^2 becomes a quadratic function of the single nuisance parameter y_0 ,

$$\chi^2(y_0) = C y_0^2 - 2B y_0 + A, \quad (2.7)$$

where A , B and C depend only on the data and on the GA reconstruction f_{GA} . Their explicit expressions are

- **Additive offset:**

$$A \equiv \sum_{i=1}^{N_{\text{data}}} \left(\frac{f_{\text{GA}}(x_i) - y_i}{\sigma_i} \right)^2, \quad B \equiv \sum_{i=1}^{N_{\text{data}}} \frac{y_i - f_{\text{GA}}(x_i)}{\sigma_i^2}, \quad C \equiv \sum_{i=1}^{N_{\text{data}}} \frac{1}{\sigma_i^2}; \quad (2.8)$$

- **Multiplicative offset:**

$$A \equiv \sum_{i=1}^{N_{\text{data}}} \left(\frac{y_i}{\sigma_i} \right)^2, \quad B \equiv \sum_{i=1}^{N_{\text{data}}} \frac{f_{\text{GA}}(x_i) y_i}{\sigma_i^2}, \quad C \equiv \sum_{i=1}^{N_{\text{data}}} \left(\frac{f_{\text{GA}}(x_i)}{\sigma_i} \right)^2. \quad (2.9)$$

Now, in order to reduce the impact of the offset, we want to marginalise y_0 . Since $\chi^2(y_0)$ is quadratic, it can be minimised analytically with respect to y_0 . One finds

$$\frac{d\chi^2}{dy_0} \stackrel{!}{=} 0, \quad \longrightarrow \quad y_0^{\text{best}} = \frac{B}{C}, \quad (2.10)$$

and the corresponding minimum value of the χ^2 is

$$\chi_{\min}^2 = A - \frac{B^2}{C}. \quad (2.11)$$

This analytical minimisation allows us to use χ_{\min}^2 , a quantity now independent on the offset y_0 , directly as the effective fitness function. This implies that the optimal constant offset is accounted for and does not need to be encoded in the chromosome. This way, GA do not have to waste generations simply to fix the offset, and for each $f_{\text{GA}}(x)$ the best y_0 is found exactly and instantaneously. This speeds up convergence and makes the comparison between different grammars more robust, since functions with the same shape but different normalisations are not artificially penalised. Moreover, different grammars can easily generate different scales, marginalising with respect to an offset reduces the possibility of the GA randomly favouring reconstructions with a normalisation closer to data, rather than reconstructions with better behaviour and representation of the underlying model. From this point on, any χ^2 appearing in the GA context will denote the marginalised quantity χ_{\min}^2 .

2.2.2 Error analysis: path-integral

A limitation of GA is that they do not provide a direct method for estimating the uncertainties of the resulting analytical function. Furthermore, the fact that the algorithm samples the function space by randomly generating function combinations can complicate the interpretation of errors associated with the best-fit. An efficient and innovative approach is therefore required to extrapolate a function $\delta f(x)$ indicative of the uncertainty along the reconstructed function $f_{\text{GA}}(x)$. While bootstrap Monte Carlo [13] offers one solution, we

adopt the approximation of the error using the *path-integral approach* from [10]. This approach is compatible with uncertainty estimation in Monte Carlo simulations, where errors are determined by sampling the parameter space around the best-fit [29]. Finally, it provides a way of obtaining an analytical, smooth, uncertainty function which can be computed in every x , analogously to $f_{\text{GA}}(x)$.

The fundamental idea is to treat the reconstructed function as the object of inference and to define a (formal) likelihood functional over the space of functions:

$$\mathcal{L}[f] \propto \exp \left[-\frac{1}{2} \chi^2[f] \right], \quad (2.12)$$

where $\chi^2[f]$ is the same goodness-of-fit functional estimator adopted in the GA. Under the assumption of Gaussian measurement errors and, in the simplest case, uncorrelated data points, the likelihood is the product of the single-point likelihoods at the sampled x_i . In this framework, the uncertainty band is constructed by determining the probability that the true function lies within an uncertainty band of half-width $\delta f(x)$ around a chosen reference reconstruction $f_{\text{GA}}(x)$:

$$f_{\text{GA}}(x) - \delta f(x) \leq f(x) \leq f_{\text{GA}}(x) + \delta f(x). \quad (2.13)$$

The path-integral construction offers a practical way to approximate this probability without explicitly resampling the dataset; it is computationally less demanding than bootstrap Monte Carlo while generating comparable confidence regions. More concretely, for each data point (x_i, y_i, σ_i) , one can introduce a confidence interval $CI(x_i, \delta f_i)$, defined as the probability (under the Gaussian likelihood) that the value of the function at x_i lies within $[f_{\text{GA}}(x_i) - \delta f_i, f_{\text{GA}}(x_i) + \delta f_i]$. For statistically independent errors, this probability can be written in closed form using error functions. The 1σ half-width is then obtained by imposing

$$CI(x_i, \delta f_i) = \text{erf} \left(\frac{1}{\sqrt{2}} \right) \simeq 0.6827, \quad (2.14)$$

which corresponds to the standard 68% confidence level of a Gaussian distribution.

If one were to determine a separate δf_i at each x_i , the resulting band would display strong point-to-point fluctuations driven by the noise in the data. To avoid this, we model $\delta f(x)$ as a smooth function (for example, a low-order polynomial $\delta f(x; \alpha, \beta, \gamma) = \alpha x^2 + \beta x + \gamma$) and fix its parameters by minimizing a functional constructed from the confidence intervals over the full dataset:

$$\chi^2_{\text{CI}}[\delta f] = \sum_{i=1}^{N_{\text{data}}} \left[CI(x_i, \delta f(x_i)) - \text{erf} \left(\frac{1}{\sqrt{2}} \right) \right]^2. \quad (2.15)$$

In practice, we constrain the solution by requiring that the perturbed reconstructions $f_{\text{GA}}(x) \pm \delta f(x)$ remain statistically consistent with the data, according to the same χ^2 metric used in the original GA fit. In this way, the final band reflects the measurement-driven statistical uncertainty encoded in the likelihood. The result is a smooth estimate of the 1σ confidence region around the GA reconstruction, obtained without the need to repeatedly rerun the GA on many mock datasets.

The path-integral result can be extended to the case where data points are correlated [25]. Following [10], one can account for correlations and incorporate the covariance matrix

and modify the χ^2 entering the GA to

$$\chi^2 = \sum_{i,j}^{N_{\text{data}}} (y_i - f(x_i)) C_{ij}^{-1} (y_j - f(x_j)), \quad (2.16)$$

where C_{ij} is the covariance matrix. For the final uncertainty estimate, the derivation follows the uncorrelated case but requires rotating the data into a basis in which they are uncorrelated (see Section II.C.2 of [10]). In this correlated framework, one obtains an analogous polynomial $\delta f_{\text{PI}}(x)$ that now incorporates the correlations between points.

In what follows, we will denote this function simply as $\delta f_{\text{PI}}(x)$, emphasizing that it represents the measurement-driven uncertainty derived via the path-integral method.

2.3 Ensemble of hyperparameter models

A sensitive point of GA is their intrinsic stochasticity and the choice of hyperparameters. The final function $f_{\text{GA}}(x)$ may differ considerably depending on the selected grammar set or on values of crossover and mutation probabilities. However, since the hyperparameter space contains elements that cannot be easily marginalised (such as the `grammar`), a standard marginalisation is not feasible. In addition, even if all hyperparameters are fixed, different random seed can still produce substantially different best-fit functions.

In order to identify the best hyperparameter setup, the typical strategy is to repeatedly run the GA with N_{conf} different hyperparameter choices and track the corresponding evolution illustrated in Figure 2.

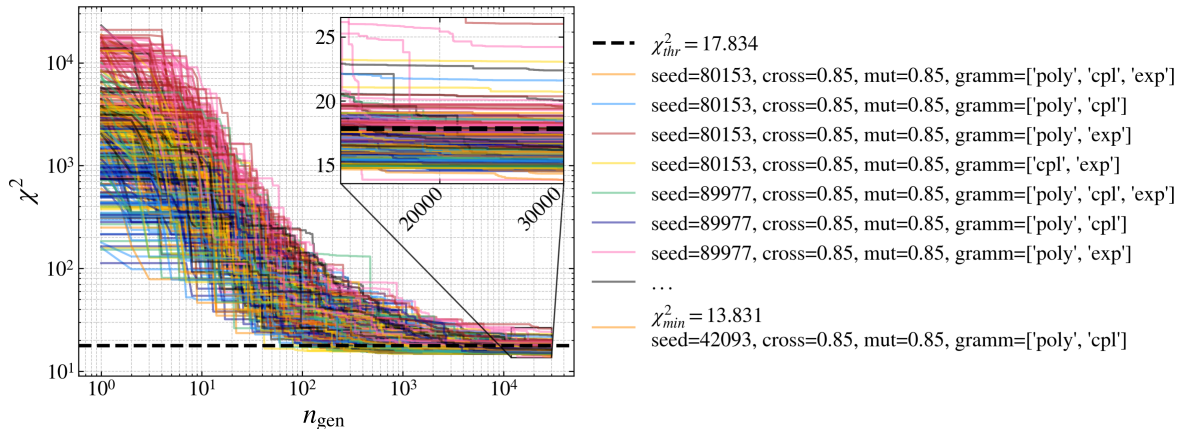


Figure 2. Evolution of the GA χ^2 with the number of generations n_{gen} . The black dotted line is the $\chi^2_{\text{threshold}}$, representing the χ^2 we aim to overcome, obtained through standard model-dependent minimisation of the parametrised function. The coloured curves represent the χ^2 of the functions generated by the GA for different configurations of the hyperparameters. In the legend each hyperparameters setup of the GA are listed.

In line with Section 2.2, once the final generation is reached, the only new ingredient is that we now have a set of N_{conf} best-fit functions. The straightforward GA prescription would be to select the single overall best-fit function, i.e. the one with the absolute minimum χ^2 . However, this result would still represent just one particularly lucky hyperparameter configuration. The selected function does not interact with the other candidates and does

not reflect the impact of hyperparameter variations. Furthermore, we cannot guarantee that choosing a different endpoint for N_{gen} would still favour the same optimal function (as suggested by Figure 2, where stopping earlier could return the best-fit of a different configuration). Since focusing only on the global minimum in χ^2 limits the potential of GA, we instead adopt a *model-averaging approach*. This strategy reduces the effects of stochasticity while incorporating multiple models across the hyperparameter space, offering greater stability for the resulting function, especially with respect to its derivatives.

2.3.1 Marginalisation over the ensemble (GAME)

We face N_{conf} different configurations, and for each configuration we obtain one best-fit function $f_{j,\text{GA}}$, forming a set of N_{conf} candidate functions (Figure 3) that we wish to combine. Since the GA output is analytical, we aim to compute a weighted average of analytic reconstructions, which acts as a representative combination of multiple GA solutions, therefore includes all the possible contributions across the hyperparameter space, including stochasticity taken into account by the random seed.

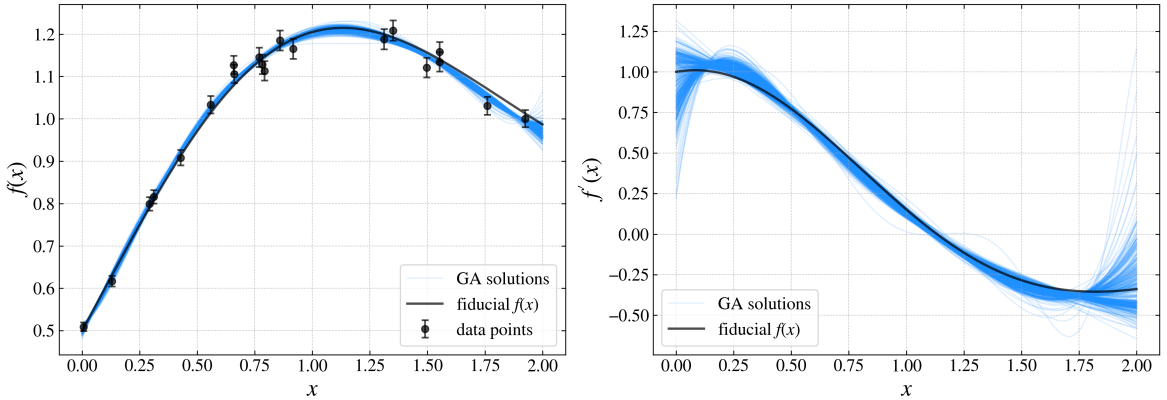


Figure 3. Ensemble of reconstructions obtained by running the GA across multiple hyperparameter configurations. *Left:* Reconstructed functions $f_{j,\text{GA}}(x)$ (blue curves) compared with the fiducial model we are trying to reproduce (black line) and the mock data points with uncertainties generated on the fiducial model. *Right:* Corresponding derivatives $f'_{j,\text{GA}}(x)$ for the same ensemble, highlighting how the spread between GA solutions grows when taking derivatives, especially near the boundaries. The collection of curves motivates a model-averaging treatment to obtain a more stable reconstructed function and derivative.

To perform averaging, we must define an estimator. A first attempt might consider the minimum χ^2 and define corresponding N_{conf} normalised weights w_j with an inverse-square or an exponential cut-off:

$$w_j = \frac{\exp\left[-\frac{1}{2}(\chi_j^2 - \chi_{\min}^2)\right]}{\sum_{k=1}^{N_{\text{conf}}} \exp\left[-\frac{1}{2}(\chi_k^2 - \chi_{\min}^2)\right]}, \quad \text{with} \quad \sum_{j=1}^{N_{\text{conf}}} w_j = 1. \quad (2.17)$$

However, this does not address the smoothness of the final function nor the fact that we are attempting to reproduce a physical quantity from statistical assumptions. A very low χ^2 does

not guarantee that the function faithfully reproduces the underlying physical model; often, it indicates overfitting, which becomes evident only when considering derivatives. Therefore, using χ^2 alone is insufficient. We define a new estimator to weigh the average and compute it for each of the N_{conf} functions:

$$S_j(\lambda) = \chi_j^2 + \lambda R_j, \quad \text{with } R_j = \int \left| f_j''(x) \right|^2 dx, \quad (2.18)$$

where R_j is the *roughness* term [30], quantifying the smoothness of the first derivative. In our implementation, this is computed numerically on the same grid used for plotting and likelihood evaluations. λ is a regularisation parameter, an arbitrary real number quantifying the relative importance of the roughness term. The lower its value, the more weight is given to the χ^2 ; conversely, the greater it is, the more the smoothness is prioritised over the data fit. Ideally, λ is fixed via a trade-off between smoothness and representativeness. We employ the *L-curve method* [31, 32], optimising the choice of regularisation parameter based on the log-log plot of the two quantities χ^2 and R . Note that we also tried to marginalise over λ by treating it as an additional hyperparameter. Although the result was consistent with the L-curve technique, this procedure was significantly slower; therefore, we chose to retain the L-curve method for reasons of computational efficiency.

To identify the optimal trade-off between χ^2 and R , we construct a cost matrix by evaluating $S_j(\lambda)$ over a dense discrete grid of $\lambda \in [10^{-5}, 10^5]$ for all N_{conf} models:

$$\begin{array}{c} \lambda \\ \hline j \left| \begin{array}{ccccc} S_1(\lambda_1) & \dots & S_1(\lambda_i) & \dots & S_1(\lambda_{\text{fin}}) \\ \vdots & \ddots & \vdots & \ddots & \vdots \\ S_j(\lambda_1) & \dots & S_j(\lambda_i) & \dots & S_j(\lambda_{\text{fin}}) \\ \vdots & \ddots & \vdots & \ddots & \vdots \\ S_{N_{\text{conf}}}(\lambda_1) & \dots & S_{N_{\text{conf}}}(\lambda_i) & \dots & S_{N_{\text{conf}}}(\lambda_{\text{fin}}) \end{array} \right. \end{array} \quad (2.19)$$

From this matrix we are able to extract the lower envelope of the model set. In practice, for each column (representing a specific λ_i), we identify the row element (representing a specific hyperparameter configuration j_*) corresponding to the minimum values of $S_j(\lambda_i)$:

$$j_*(\lambda_i) = \arg \min_{j \in 1, \dots, N_{\text{conf}}} S_j(\lambda_i). \quad (2.20)$$

By scanning the λ grid results of S_j in the matrix (2.19), and then locating $S_{j_*}(\lambda_i)$, it is possible to identify and collect for each λ_i the corresponding pair $\chi_{j_*}^2$ and R_{j_*} associated with the minimum, i.e., the optimal pair configuration that produces the best S at a given λ :

$$S_{\min}(\lambda) = S_{j_*}(\lambda), \quad \rightarrow \quad (R_{j_*(\lambda)}, \chi_{j_*(\lambda)}^2). \quad (2.21)$$

Note that many different values of λ_i can correspond to the same optimal model j_* (i.e., as we vary λ , we may keep obtaining the same index j_* and the same corresponding minimum value S_{j_*}). The reason is that, with χ_j^2 fixed, minimising the sum with λR_j often produces only a limited number of distinct S_{\min} values, making the outcome quite sensitive to the step size chosen for λ . As a result, the full scan effectively identifies only a relatively small subset of configurations that are effectively *active* in the trade-off. This process filters the ensemble

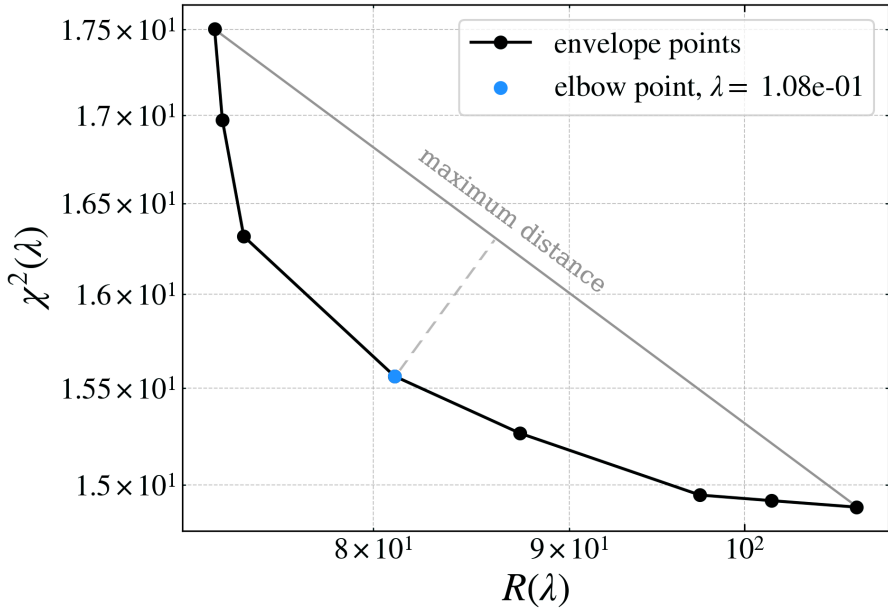


Figure 4. L-curve used to identify the optimal regularization parameter λ for the estimator $S_j(\lambda) = \chi_j^2 + \lambda R_j$. Black markers represent the lower-envelope points $(R_{j_*}, \chi_{j_*}^2)$ obtained by scanning the λ grid and identifying the specific configuration j_* that minimizes S_j at each step. These points represent the active subset of the N_{conf} ensemble; their limited number indicates that many λ values map to the same optimal model j_* . The blue marker identifies the elbow point, defined by the maximum curvature in the log R -log χ^2 plane, where the trade-off between goodness-of-fit (χ^2) and smoothness (R) is optimized. This determines λ_{elbow} , which is subsequently used to calculate the exponential weights w_j for the final model-averaging procedure.

down to the small subset of models that are optimal for at least one value of λ . The pairs $(R_{j_*}, \chi_{j_*}^2)$ corresponding to this subset are then plotted to form the L-curve in Figure 4.

The L-curve method involves choosing the regularisation parameter λ at the point where the curve exhibits the largest bending in the log-log space (the so-called *elbow*) [31, 32]. This point represents the optimal trade-off, marking the transition between the regime driven mainly by χ^2 (small λ), where the model fits the noise, and the regime dominated by the regularity constraint (large λ), where the actual signal begins to be smoothed. It serves as a criterion to select a regularisation parameter introduced without any prior. In practice, after collecting and ordering the envelope points by increasing R , we work in log-log space and identify the elbow as the point of maximum distance from the straight line connecting the two endpoints of the envelope.

This produces a characteristic configuration j_{elbow} and an associated representative value λ_{elbow} , chosen within the range of λ for which j_{elbow} minimises $S_j(\lambda)$. Once λ_{elbow} is fixed, we define the weights w_j through S_j :

$$w_j(\lambda_{\text{elbow}}) = \frac{\exp\left[-\frac{1}{2}(S_j(\lambda_{\text{elbow}}) - S_{\min}(\lambda_{\text{elbow}}))\right]}{\sum_{k=1}^{N_{\text{conf}}} \exp\left[-\frac{1}{2}(S_k(\lambda_{\text{elbow}}) - S_{\min}(\lambda_{\text{elbow}}))\right]}, \quad (2.22)$$

which corresponds to an exponential cut-off driven by the combined estimator S . We can interpret this estimator not only as a likelihood (χ^2) but as a posterior with regularisation prior (λR).

The averaged analytical function is then computed as a weighted sum of the symbolic N_{conf} best-fit solutions of the GA:

$$f_{\text{GAME}}(x) = \sum_{j=1}^{N_{\text{conf}}} w_j(\lambda_{\text{elbow}}) \cdot f_{j,\text{GA}}(x). \quad (2.23)$$

2.3.2 Error analysis: ensembling and total uncertainty

The model-averaging described above mitigates the intrinsic stochasticity and the impact of hyperparameters setup of the GA. However, working with an averaged reconstruction requires an upgrade in the uncertainty estimation: besides the measurement-driven statistical uncertainty on the resulting function ($\delta f_{\text{PI}}(x)$), we must account for an additional configuration-driven spread, that is the dispersion among the different GA best-fit functions entering the ensemble (σ_{ens}).

For the former, we quantify the statistical uncertainty around the reconstructed function using the path-integral approach described in Section 2.2.2. In the averaged scenario, we adopt the weighted-mean reconstruction $f_{\text{GAME}}(x)$ and generate a smooth error band by imposing the 1σ confidence interval condition. The function $\delta f_{\text{PI}}(x)$ encodes the uncertainty implied by the likelihood functional $\mathcal{L}[f] \propto \exp[-\chi^2[f]/2]$.

For the latter, we consider the set of best-fit GA reconstructions $f_{j,\text{GA}}$ and the associated weights w_j , evaluated at λ_{elbow} , obtaining the weighted-averaged analytical function given in Equation (2.23). At each x , we define a weighted ensemble variance as a quantitative measure of the remaining configuration uncertainty [33]:

$$\sigma_{\text{ens}}^2(x) = \sum_{j=1}^{N_{\text{conf}}} w_j(\lambda_{\text{elbow}}) \left(f_{j,\text{GA}}(x) - f_{\text{GAME}}(x) \right)^2, \quad (2.24)$$

which quantifies how much the reconstructions fluctuate around the averaged solution when scanning the hyperparameters space. Note that $\sigma_{\text{ens}}(x)$ is tied to the stability of the reconstruction procedure itself rather than the measurement errors of a single run.

Finally, we combine the two contributions into a single effective 1σ band. Since the measurement noise (captured by δf_{PI}) and the stochastic nature of the GA (quantified by σ_{ens}) are uncorrelated processes, we treat them as independent sources of error and therefore sum their variances in quadrature:

$$\sigma_{\text{tot}}^2(x) = \delta f_{\text{PI}}^2(x) + \sigma_{\text{ens}}^2(x), \quad \longrightarrow \quad f_{\text{GAME}}(x) \pm \sigma_{\text{tot}}(x), \quad (2.25)$$

This provides a conservative and numerically stable error estimate. Here, $\delta f_{\text{PI}}(x)$ is computed for the final averaged reconstruction $f_{\text{GAME}}(x)$ (representing the statistical measurement uncertainty driven by the data likelihood), independent on the N_{conf} explored. In contrast, $\sigma_{\text{ens}}(x)$ inflates the error band in regions where different GA configurations produce significantly different functional behaviours, that is particularly relevant for derivatives as seen in Figure 3.

The same logic applies to derived quantities such as $f'(x)$. We compute the analytical derivative for each model, then build the weighted-averaged derivative:

$$f'_{\text{GAME}}(x) = \sum_{j=1}^{N_{\text{conf}}} w_j(\lambda_{\text{elbow}}) \cdot f'_{j,\text{GA}}(x), \quad (2.26)$$

and define the corresponding weighted ensemble variance for the derivative:

$$\sigma_{\text{ens}}^2[f'(x)] = \sum_{j=1}^{N_{\text{conf}}} w_j(\lambda_{\text{elbow}}) \left(f'_{j,\text{GA}}(x) - f'_{\text{GAME}}(x) \right)^2. \quad (2.27)$$

For the path-integral contribution δf_{PI} , we propagate the uncertainty by differentiating the reconstruction band. This assumes that the variation operator δ commutes with the derivative:

$$\delta \left(\frac{df}{dx} \right) = \frac{d}{dx} \delta f(x). \quad (2.28)$$

While this commutation is not generally true for arbitrary distributions, it is consistent with the Gaussian likelihood approximation ($\mathcal{L} \propto e^{-\chi^2/2}$) employed in the path-integral framework (Section 2.2.2). Under this approximation, the perturbations are treated as linear fluctuations around the best-fit, allowing for standard error propagation [25].

The final 1σ uncertainty on the derivative of the **GAME** function is obtained analogously to Equation (2.25):

$$\sigma_{\text{tot}}^2[f'(x)] = \delta f_{\text{PI}}^2(x) + \sigma_{\text{ens}}^2[f'(x)], \quad \rightarrow \quad f'_{\text{GAME}}(x) \pm \sigma_{\text{tot}}[f'(x)]. \quad (2.29)$$

2.3.3 Improvements in the reconstruction

Finally, we fix the different N_{conf} hyperparameters configurations (Appendix B) and feed the algorithm with the mock data. It generates a set of candidates from which we identify the standard best-fit **GA** function $f_{\text{GA}}(x)$ (corresponding to the minimum χ^2 between all the configurations) and compute the **GAME** averaged function $f_{\text{GAME}}(x)$ with its associated total uncertainty. We then compare the reconstructions obtained via the two methodologies.

In Figure 5, we observe that for the reconstruction of $f(x)$, both methodologies generate analytical functions that are compatible at the 1σ level. However, **GAME** reconstruction tends to be more stable and resistant to overfitting. To rigorously quantify this improvement, we introduce the cumulative statistic $\tilde{\chi}_{\text{tot}}^2 = \sum_x [(f_{\text{fid}}(x) - f_{\text{GA}}(x)) / \sigma_{\text{tot}}(x)]^2$. This estimator serves as a metric to evaluate and compare how well the reconstructions reproduce the underlying target model³ $f(x)$. In Figure 6, we observe the evolution of the cumulative $\tilde{\chi}_{\text{tot}}^2$ for both the function and its derivative. While the improvement for $f(x)$ is visually subtle in the reconstruction plots, the cumulative estimator reveals a quantitative improvement of $\sim 20\%$.

For the derivative $f'(x)$, the advantage of the **GAME** approach is evident. As seen in the right panel of Figure 5, the differentiated **GA** best-fit is inaccurate at both low and high values of x despite having the global minimum χ^2 on the data. Instead, by applying **GAME** and weighting the ensemble with an estimator sensitive to roughness, makes the derivative significantly more stable, with an uncertainty that accounts for major deviations (in this case, at low and high x values), and achieving an improvement of $\sim 95\%$.

³The tilde \sim is introduced to distinguish this model-function χ^2 from the data-function χ^2 used within the **GA** (Equation (2.1)).

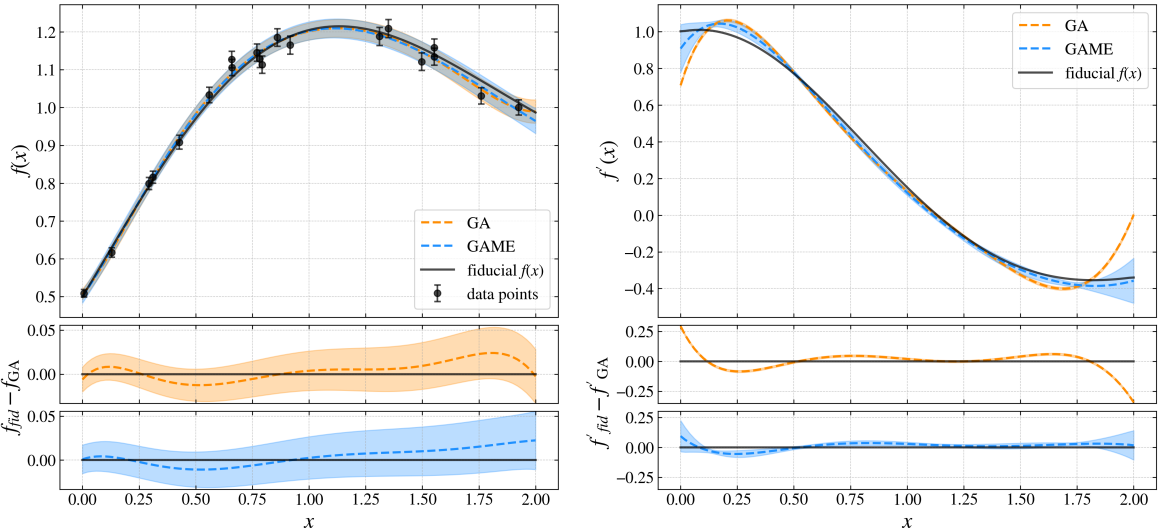


Figure 5. Comparison of function reconstruction and derivative estimation between the standard GA and GAME methodologies. The bottom sub-panels display the residuals for the GA and GAME methods, respectively. *Left:* Reconstruction of the function $f(x)$. The solid black line indicates the underlying fiducial function (Equation (2.6)) we are trying to reproduce from the mock dataset. The orange dashed line shows the standard best-fit GA result, while the blue dashed line represents the GAME averaged reconstruction. Shaded regions indicate 1σ confidence intervals. *Right:* Derivation of the derivative $f'(x)$. While the reconstructed functions f_{GA} and f_{GAME} are comparable, the derivative estimation highlights the stability of the GAME averaging at the boundaries ($x \approx 0$ and $x \approx 2$), where the standard GA deviates significantly from the fiducial line.

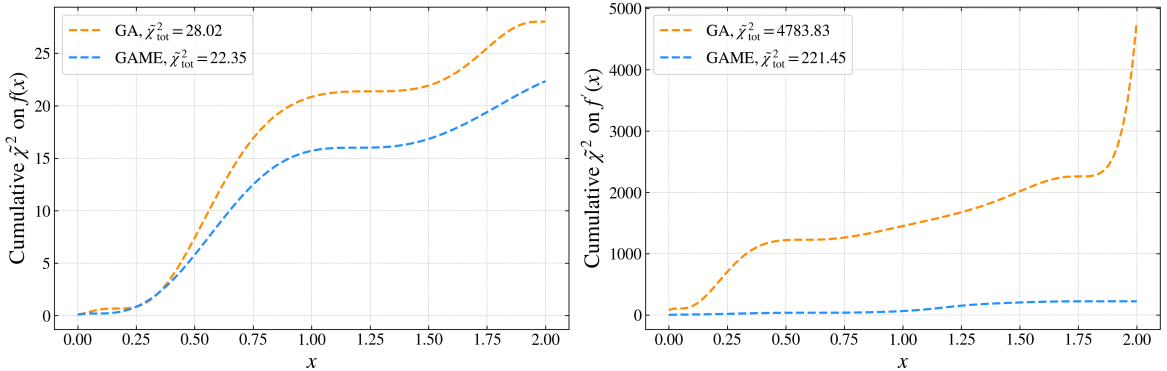


Figure 6. Cumulative performance of the reconstruction methodologies against the true fiducial model. The panel show the cumulative $\tilde{\chi}_{\text{tot}}^2$ as a function of x , calculated between the reconstructed function and the underlying target model, normalised by the total uncertainty σ_{tot} . *Left:* Cumulative $\tilde{\chi}_{\text{tot}}^2$ for the function $f(x)$. The blue line (GAME approach) reaches a final value of $\tilde{\chi}_{\text{tot}}^2 \approx 22$, representing a $\sim 20\%$ improvement over the orange line (standard GA best-fit) $\tilde{\chi}_{\text{tot}}^2 \approx 28$. *Right:* Cumulative $\tilde{\chi}_{\text{tot}}^2$ for the derivative $f'(x)$. Here the difference is drastic: the standard GA accumulates a massive error at the boundaries due to instability ($\tilde{\chi}_{\text{tot}}^2 \approx 4783$), while GAME maintains stability throughout ($\tilde{\chi}_{\text{tot}}^2 \approx 221$) resulting in a $\sim 95\%$ improvement in accuracy.

This test confirms that the **GAME** methodology has the potential to reconstruct generic functions and derived quantities in a non-parametric and model-independent manner. We proceed by applying **GAME** to cosmological quantities and real data to assess the quality of such reconstructions and their ability to constrain cosmological parameters.

3 Application to cosmological quantities

3.1 Dark energy equation of state

We aim to test the standard Λ CDM model through dark energy, which is not a directly observable quantity. One can study its equation of state w using direct observations of background quantities such as the luminosity distance of Type Ia supernovae $D_L(z)$, or the expansion rate of the universe, $H(z)$. From $H(z)$, w can be derived following parametric or non-parametric approaches [34]. We assume the universe is well described by an FLRW metric and consider a Friedmann equation for a late-time flat universe containing only matter and dark energy (neglecting radiation at low redshifts):

$$\frac{H(z)^2}{H_0^2} = \Omega_{m,0}(1+z)^3 + \Omega_{\text{de}}(z), \quad \text{with} \quad \Omega_{\text{de}}(z) = \rho_{\text{de}}(z) \frac{8\pi G}{3H(z)^2}. \quad (3.1)$$

Assuming dark energy acts as a perfect fluid ($p_{\text{de}} \equiv w(z)\rho_{\text{de}}$), and as a non-interacting fluid ($\dot{\rho}_{\text{de}} + 3H(1+w)\rho_{\text{de}} = 0$), we obtain [9]:

$$w(z) = -1 + \frac{1}{3}(1+z) \frac{d \ln \left(\frac{H(z)^2}{H_0^2} - \Omega_{m,0}(1+z)^3 \right)}{dz}. \quad (3.2)$$

This expression links the evolving dark energy equation of state to background evolution quantities. By reconstructing $H(z)$ from data and assuming a prior value for $\Omega_{m,0}$, we can perform a consistency check with the expected Λ CDM value ($w = -1$).

However, Equation (3.2) is derived under the assumptions of a flat FLRW geometry and the GR theory of gravity. If any of these assumptions is violated ($\Omega_k \neq 0$ or modified gravity affecting Friedmann equations), then the reconstructed $w(z)$ ceases to measure the physical properties of the dark energy fluid alone. Instead, it absorbs the effects of curvature and modified gravity, making them mathematically indistinguishable from a change in the dark energy equation of state.

Within this framework, any deviation from $w = -1$ can imply one of these physical scenarios [8]:

- **Dynamical dark energy:** the fluid is not a vacuum energy density but a dynamical field with a time-evolving equation of state [35].
- **Interacting dark energy:** our derivation assumes the continuity equation. If there is an energy exchange between dark matter and dark energy, this interaction can mimic an effective equation of state $w(z) \neq -1$ even if the fluid itself is a cosmological constant [36].
- **Matter density parameter bias:** the reconstruction of $w(z)$ is mathematically degenerate with the matter density parameter. An incorrect prior on $\Omega_{m,0}$ will induce a spurious evolution in $w(z)$ to compensate for the density mismatch [37].

In order to disentangle the dark energy sector from the systematic parameter bias (scenario 3), we frame the current observational landscape by computing $w(z)$ using two distinct priors on $\Omega_{m,0}$:

- **Planck 2018** [38]: $\Omega_{m,0} = 0.315 \pm 0.007$, representing the CMB constraints.
- **DESI DR1** [39]: $\Omega_{m,0} = 0.295 \pm 0.015$, representing recent constraints from Baryonic Acoustic Oscillations (BAO).

3.2 Testing Λ CDM with current data surveys

To derive $w(z)$, we must reconstruct $H(z)$. A known issue is that any possible data relating the two quantities must be differentiated at least once. Distance data, such as Type Ia supernovae, require two derivatives [35], greatly enhancing the error on $w(z)$. Following [8], we utilise direct measurements of $H(z)$ from CC. Although these observations are sparser and much more affected by systematics, they require only one derivative (see Equation (3.2)), making them good candidates to apply **GAME** methodology. CC are based on massive, passively evolving early-type galaxies that act as standard clocks. By measuring the differential age evolution dt between two such galaxies separated by a small redshift interval dz , one can directly determine the expansion rate via the relation $H(z) = -\frac{1}{1+z} \frac{dz}{dt}$. Particularly, the dataset we have used comes from Table 1 of [40], at which we have added a recent measurement from [41]. Unlike luminosity distance, this method measures the Hubble rate directly, allowing for a determination of the expansion history that does not rely on integrations over the equation of state $w(z)$ [42].

3.2.1 Reconstruction of $H(z)$

We first fix the hyperparameters configurations (Appendix B), then we feed the GA with CC data to reconstruct $H(z)$. We consider a dataset of measurements at $z \lesssim 2$. Even though some of these data points are known to be correlated [43], we treat the sample as uncorrelated to perform an additional robustness test, with the objective of remaining as agnostic as possible in order to test the goodness of the methodology. Including correlations inject extra information and, as seen in Section 2.2.2, correlated data just impact the value of the χ^2 entering the GA (Equation (2.16)). In case we wanted to build a covariance matrix for the CC $H(z)$ measurements, this could be done following the procedure described in [43].

Once the GA has converged, we identify the global minimum χ^2 best-fit solution, $H_{\text{GA}}(z)$, and then calculate H_{GAME} using the **GAME** weighted-averaged approach described in Section 2.3.1. Figure 7 presents a comparison of the reconstructed $H(z)$ and $H'(z)$ obtained from the standard minimum best-fit function selection and from the **GAME** approach.

Both methods provide a good reconstruction of $H(z)$, although **GAME** appears slightly more stable at higher redshifts. For the derivative $H'(z)$, **GAME** derivation is significantly more consistent with Λ CDM than the standard GA result. Because GA is primarily driven by the χ^2 statistic, we also observed that excluding data points with larger uncertainty bands σ_i substantially enhances the reconstruction quality, in particular its constraining ability and the behaviour of δf_{PI} (Appendix A).

3.2.2 Derivation of $w(z)$

Using Equation (3.2), we derive the evolution of the dark energy equation of state $w(z)$ under the assumptions of GR and a flat FLRW metric. This derivation is particularly challenging

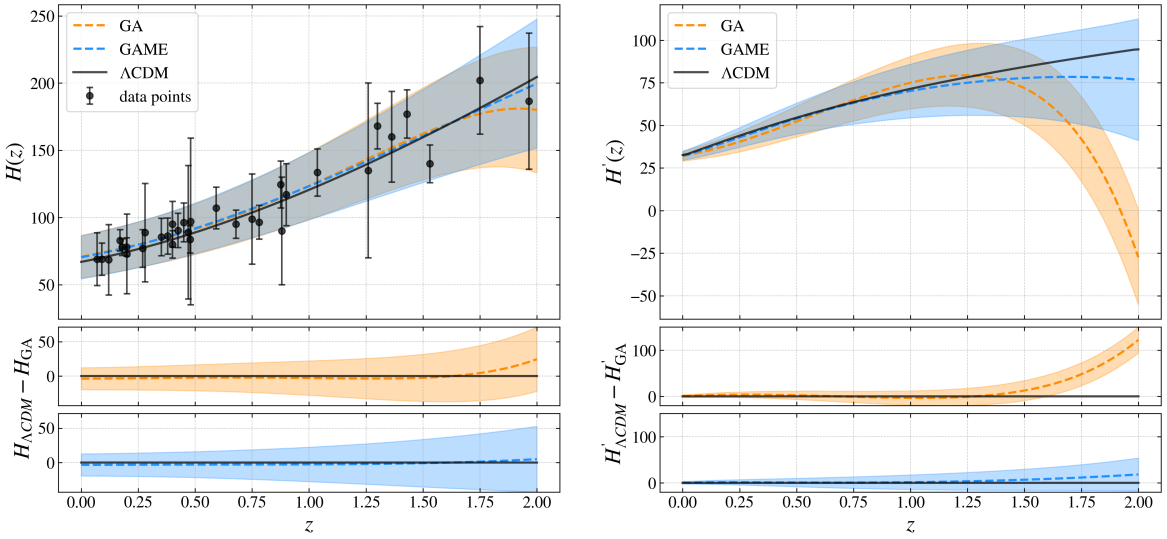


Figure 7. Comparison of $H(z)$ reconstruction and derivative estimation between the standard GA and GAME methodologies using CC data. *Left:* Reconstruction of the Hubble parameter $H(z)$. The solid black line indicates the flat Λ CDM model. The orange dashed line shows the standard best-fit GA result, while the blue dashed line represents the GAME marginalised-ensemble reconstruction. Shaded regions between dotted lines indicate 1σ confidence intervals. *Right:* The corresponding reconstruction of the derivative $H'(z)$. While the function reconstructions (left) are largely consistent, the derivative reconstruction highlights the enhanced stability of the GAME method (blue), which provides a smoother evolution compared to the standard GA (orange) that exhibits more pronounced fluctuations, particularly at higher redshifts.

because it requires not only the function $H(z)$ but also its first derivative $H'(z)$, making it highly sensitive to the smoothness of the reconstruction. We utilise the H_{GAME} and H'_{GAME} profiles obtained from the marginalised ensemble of CC data to compute $w(z)$ assuming the two priors on $\Omega_{m,0}$ listed in 3.1. The uncertainties on $w(z)$ are computed via standard error propagation, combining the variance from GAME reconstruction (σ_H) with the reported uncertainties on $\Omega_{m,0}$.

Figure 8 shows the estimate evolution of $w(z)$. At low redshifts ($z \lesssim 1$), where dark energy dominates the total energy budget, the reconstruction is robust and tightly constrained. Regardless of the assumed prior on $\Omega_{m,0}$, the results are in excellent agreement with the standard Λ CDM expectation ($w = -1$). At higher redshifts ($z \gtrsim 1.5$), however, the confidence regions begin to diverge significantly, indicating a loss of constraining power. This behavior is intrinsic to non-parametric derivations of $w(z)$ in a spatially flat universe. In such frameworks, the equation of state is determined by the logarithmic derivative of the dark energy density, $d \ln \Omega_{\text{de}}/dz \propto \Omega'_{\text{de}}/\Omega_{\text{de}}$. As we approach the matter-dominated era ($z \gtrsim 1.5$), $\Omega_{\text{de}}(z)$ is obtained as the difference between the total expansion rate and the matter contribution: $\Omega_{\text{de}}(z) \approx H(z)^2/H_0^2 - \Omega_{m,0}(1+z)^3$. In this regime, that difference tends to zero ($\Omega_{\text{de}} \rightarrow 0$), causing the logarithm in the expression for $w(z)$ toward infinity. Consequently, even tiny stochastic fluctuations in the reconstructed $H(z)$ or small deviations in $\Omega_{m,0}$ can generate apparent singularities, leading to the massive expansion of the confidence intervals at high redshift.

Despite the loss of constraining power at high z , GAME methodology produces a robust

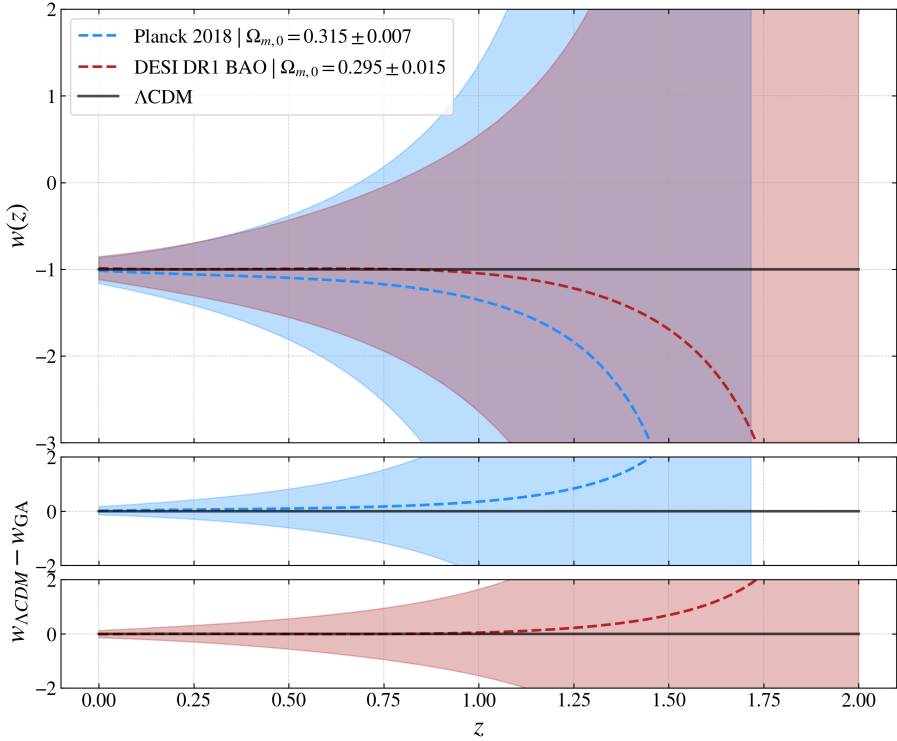


Figure 8. Optimised estimation of the dark energy equation of state $w(z)$ derived from the GAME-reconstructed $H(z)$ using CC data. The derivation assumes a flat FLRW metric and is performed for two different priors on the matter density parameter $\Omega_{m,0}$. The solid black line indicates the standard Λ CDM value ($w = -1$). The blue dashed line represents the derivation assuming the Planck 2018 CMB prior, while the red dashed line assumes the DESI DR1 BAO prior. Shaded regions indicate the 1σ uncertainty bands obtained via error propagation. At low redshifts ($z \lesssim 1$), both derivations produce tight constraints compatible with the cosmological constant. At higher redshifts, the reconstruction becomes highly sensitive to the assumed matter density and the sparsity of the data, leading to a significant widening of the uncertainty bands and a divergence, though remaining statistically consistent with Λ CDM.

estimate of the present-day equation of state. Adopting the DESI prior on $\Omega_{m,0}$, which favors a lower matter density, we obtain our tightest constraint:

$$w(0) = -0.986 \pm 0.132. \quad (3.3)$$

This measurement confirms that, with current CC data, the local universe remains fully compatible with a cosmological constant. The apparent deviation from Λ CDM observed in the reconstruction at high z is not statistically meaningful given the large uncertainties, but it highlights the critical importance of precise $H(z)$ measurements and accurate local matter density priors for extending dark energy tests into the matter dominated era.

3.3 Forecasts with future data surveys

To further validate the GAME methodology, we test its robustness using mock data that emulate the characteristics of next generation cosmological surveys. We assume a standard fiducial cosmological model (Λ CDM) and generate a simulated dataset that reflects the data density and precision expected from Stage IV surveys (such as Euclid [44] or high-precision

releases from DESI [45]). This is the crucial step: if **GAME** can accurately recover the underlying function and its derivative from noisy synthetic data, without generating artificial features, it confirms the method’s reliability for applications in the precision cosmology era.

3.3.1 Reconstruction of $H(z)$

We generate a mock catalog for $H(z)$ consisting of $N_{\text{data}} = 15$ points distributed between redshift 0 to 2. To emulate realistic observational conditions, we adopt a redshift-dependent uncertainty on the measurement given by $\sigma_H(z) = 2\%(1 + z) H(z)$, using a conservative 2% error factor. This choice captures the typical loss of precision at higher redshifts found in spectroscopic surveys [44]. We examined both uniformly spaced and randomly sampled redshift distributions and obtained comparable results; in what follows, we show the results for the uniform case.

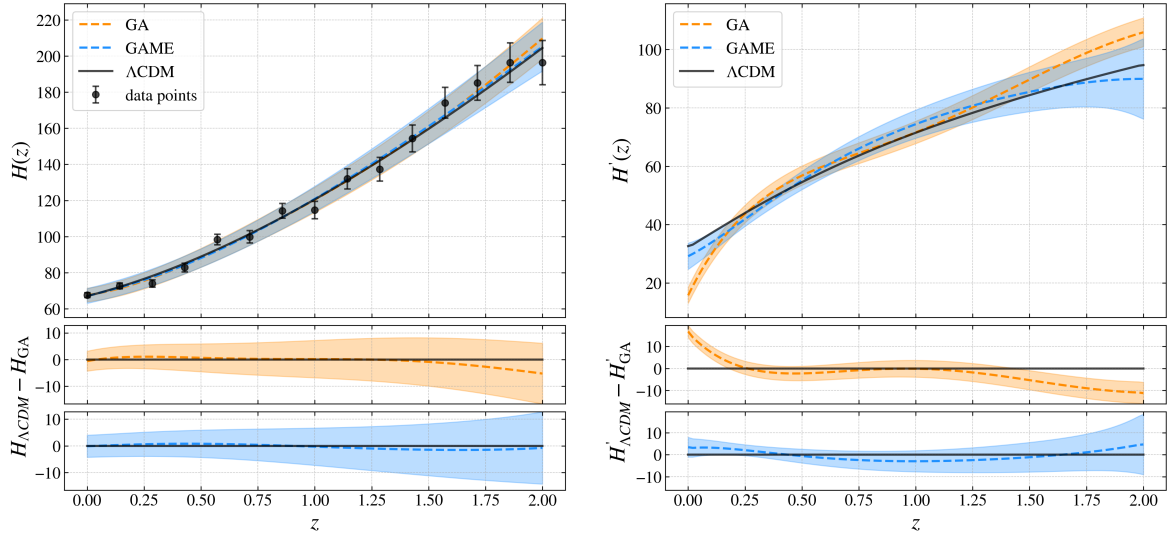


Figure 9. Comparison of $H(z)$ reconstruction and derivative estimation between the standard GA and **GAME** methodologies using a synthetic Stage IV-like dataset. *Left:* Reconstruction of the Hubble parameter $H(z)$ from 15 mock data points generated on a flat Λ CDM fiducial (solid black line). The points include a measurement uncertainty of $2\%(1 + z)$. The orange dashed line shows the standard best-fit GA result, while the blue dashed line represents the **GAME** averaged reconstruction. Shaded regions indicate 1σ confidence intervals. *Right:* The corresponding estimate of the derivative $H'(z)$. As observed with real data (Figure 7), **GAME** reconstruction maintains the expected smoothness in the derivative $H'(z)$, successfully recovering the Λ CDM fiducial without the high-redshift oscillations present in the single best-fit GA run.

Figure 9 compares the reconstruction of $H(z)$ and its derivative $H'(z)$ using the standard GA best-fit versus the **GAME** averaged function. Both methods successfully reconstruct the Hubble parameter $H(z)$, closely following the fiducial Λ CDM line. Once again, the strength of the **GAME** methodology becomes apparent in the derivative. Symbolic regression techniques can be sensitive to local noise, often resulting in oscillations in the derivative $H'(z)$ even when $H(z)$ appears smooth but **GAME** reconstruction effectively suppresses these oscillations, reproducing the fiducial derivative more faithfully than the single GA best-fit, particularly at the boundaries ($z \approx 0$ and $z \approx 2$).

As for the test function $f(x)$ in Section 2.3.3 we quantify this improvement in stability by computing the cumulative statistic $\tilde{\chi}_{\text{tot}}^2$. In Figure 10 we show the evolution of the cumulative $\tilde{\chi}_{\text{tot}}^2$ for both $H(z)$ and $H'(z)$. For $H(z)$ the improvement is visually subtle in

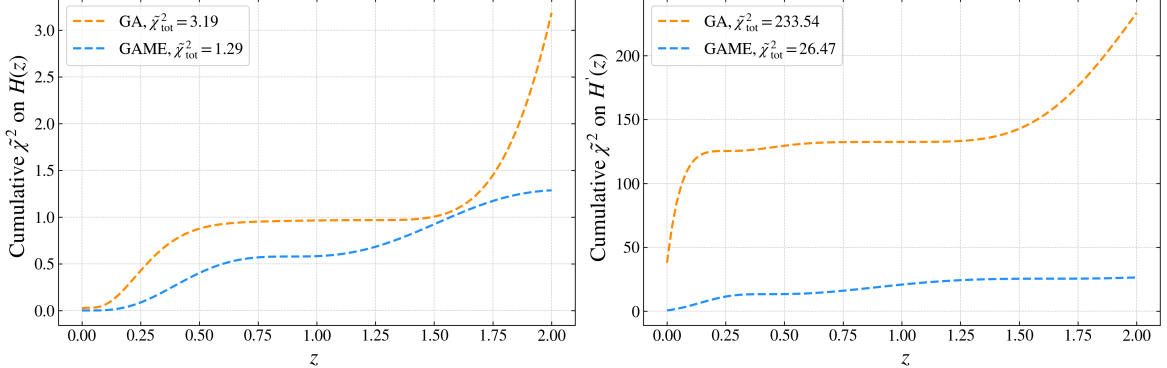


Figure 10. Cumulative performance of the reconstruction methodologies against the assumed fiducial model (Λ CDM). The panels show the cumulative $\tilde{\chi}_{\text{tot}}^2$ as a function of redshift z , calculated between the reconstructed functions and the underlying target model. *Left:* Cumulative $\tilde{\chi}_{\text{tot}}^2$ for the Hubble rate $H(z)$. The blue line (GAME approach) reaches a final value of $\tilde{\chi}_{\text{tot}}^2 = 1.29$, representing a $\sim 60\%$ improvement over the orange line (standard GA best-fit, $\tilde{\chi}_{\text{tot}}^2 = 3.19$). *Right:* Cumulative $\tilde{\chi}_{\text{tot}}^2$ for the derivative $H'(z)$. Here the advantage of the proposed method is more clear: the standard GA accumulates large errors due to instability ($\tilde{\chi}_{\text{tot}}^2 = 233.54$), while GAME maintains robustness ($\tilde{\chi}_{\text{tot}}^2 = 26.47$), resulting in a $\sim 89\%$ improvement in accuracy.

the reconstruction plot, but the cumulative estimator reveals a quantitative gain of $\sim 60\%$, with $\tilde{\chi}_{\text{tot}}^2$ decreasing from $\tilde{\chi}_{\text{tot,GA}}^2 = 3.19$ to $\tilde{\chi}_{\text{tot,GAME}}^2 = 1.29$. For the derivative $H'(z)$ the advantage of the GAME approach is much clearer, achieving an improvement of $\sim 89\%$, as $\tilde{\chi}_{\text{tot}}^2$ is reduced from $\tilde{\chi}_{\text{tot,GA}}^2 = 233.54$ to $\tilde{\chi}_{\text{tot,GA}}^2 = 26.47$. Besides representing a substantial improvement and notable increase in the reliability of recovering the underlying physical models, this refined stability is essential for deriving the equation of state $w(z)$, which depends directly on the gradient of the expansion history.

3.3.2 Derivation of $w(z)$

Using the GAME-reconstructed $H(z)$ and $H'(z)$ from the mock dataset, we compute the dark energy equation of state $w(z)$ by applying the same procedure described in Section 3.2.2. Since the mock observations are generated under a Λ CDM model with $w = -1$, this acts as a null test for our pipeline: we verify whether the algorithm introduces any systematic bias or signatures of dynamical dark energy. Figure 11 shows the resulting $w(z)$ obtained adopting the same priors on $\Omega_{m,0}$ as those used for the derivation with real data. The reconstruction is fully consistent with the fiducial value $w = -1$ across the entire redshift range. The uncertainty bands naturally widen at higher redshifts due to the combined effects of the error propagation in Equation (3.2) and the decreasing relative importance of dark energy relative to matter. Most notably, the constraint at $z = 0$ is significantly improved compared to what is obtainable with current CC measurements. Assuming Planck prior for $\Omega_{m,0}$, we obtain a precise estimate of the present-day equation of state:

$$w(0) = -1.037 \pm 0.051. \quad (3.4)$$

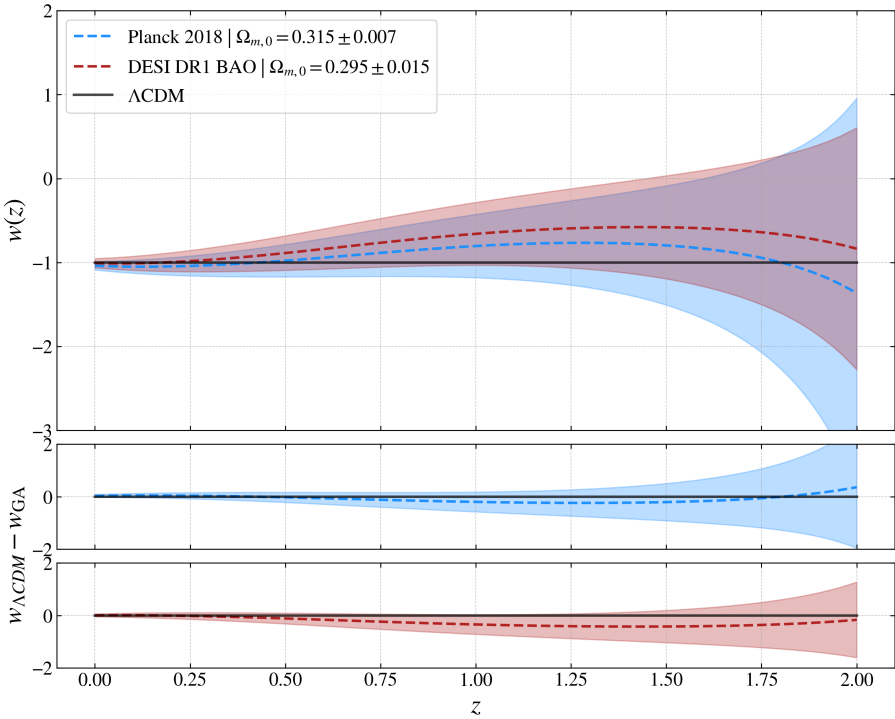


Figure 11. Optimised reconstruction of the dark energy equation of state $w(z)$ derived from the GAME-reconstructed mock $H(z)$. The derivation assumes a flat FLRW metric and is performed for two different priors on the matter density parameter $\Omega_{m,0}$. The solid black line indicates the input fiducial Λ CDM model ($w = -1$). The blue dashed line represents the derivation assuming the Planck prior, while the red dashed line assumes the DESI DR1 BAO prior. Shaded regions indicate the 1σ uncertainty bands obtained via error propagation. The reconstruction successfully recovers the fiducial value $w = -1$ within 1σ over the entire redshift range. Notably, the constraints at $z = 0$ are significantly tighter than those obtained from current data, demonstrating the potential of GAME to leverage the precision of future surveys.

This result represents a factor of ~ 2.6 improvement in precision compared to the result obtained from current data in Section 3.2.2. This test confirms that GAME is not only capable of unbiased reconstruction, but it is also ready to exploit the higher statistical power of upcoming Stage IV datasets to place tight, non-parametric constraints on the nature of dark energy, regardless of the prior on $\Omega_{m,0}$.

4 Conclusions and outlook

In this paper, we proposed GAME: an update to the standard GA methodology for model-independent reconstructions of cosmological functions. While GA provide a powerful symbolic regression framework independent of specific parametrisations, a known weakness is the sensitivity of derived quantities (especially those involving derivatives) to stochasticity and hyperparameter choices. This sensitivity can lead to reconstructions that fit the data equally well but generate noticeably different derivatives, affecting consistency tests based on derived quantities like the dark energy equation of state $w(z)$.

To mitigate these issues, we introduced a model-averaging approach over an ensemble of GA best-fit reconstructions (GAME). We defined weights using a combined estimator

$S_j = \chi_j^2 + \lambda R_j$ (where R_j is a roughness penalty) and selected the regularisation scale λ via an L-curve method. The final reconstruction is the weighted average of all the analytical GA solutions associated to different hyperparameters configurations, improving stability and reducing overfitting in derivative-dependent observables. Consequently, we updated the uncertainty estimation to match the averaged framework by combining a measurement error component (estimated through a path-integral uncertainty estimation) with an ensemble error contribute (estimated through the weighted variance across configurations), constructing a conservative total uncertainty.

This updated methodology also benefits from the significant increase in computational power available since the introduction of GA in cosmology. While early applications were often limited to $\mathcal{O}(10^3)$ generations and a single configuration due to CPU constraints, modern resources allow us to routinely exceed this by one or two orders of magnitude and by also exploring many configurations at the same time. This deeper exploration of the functional space, combined with our ensemble averaging, substantially improves the convergence of the algorithm and reduces the risk of settling in local minima.

We validated the method on a controlled example function $f(x)$, demonstrating that the marginalised ensemble reconstruction. Using a $\tilde{\chi}^2$ statistic against the true fiducial model, we quantified an improvement of $\sim 20\%$ in the reconstruction of the function itself and a substantial $\sim 95\%$ improvement in the accuracy of the derivative, highlighting the ability of **GAME** to reproduce underlying models. We then applied **GAME** to current CC data, reconstructing $H(z)$ and its derivative, and derived $w(z)$ under FLRW and GR assumptions for different priors on $\Omega_{m,0}$. Within uncertainties, the reconstructed $w(z)$ is compatible with Λ CDM at low redshift. The loss of constraining power at higher redshift naturally widens the bands, highlighting the limitations of sparse $H(z)$ measurements, their precision, and the importance of stable derivative reconstruction.

Finally, we explored forecasts with Stage IV-like mock datasets. Even with a conservative error factor assumption, and while we keep using the same priors on $\Omega_{m,0}$, **GAME** recovers the fiducial Λ CDM behaviour with improved stability and produces a significantly tighter reconstruction of $w(z)$ at low redshift compared to present data. This illustrates the potential of GA reconstructions, when properly marginalised, to become a competitive tool for model-independent consistency tests with upcoming surveys.

Several natural extensions of this work are possible. On the data side, a key next step is to incorporate the full covariance structure of CC (and other probes) directly into the GA likelihood, in order to assess and quantify the impact of data correlations. On the theoretical side, one can broaden the consistency analysis by relaxing assumptions such as spatial flatness and by jointly reconstructing multiple background and perturbation observables, enabling more direct tests of gravity and of the associated underlying theories. Taken together, **GAME** offers a practical and adaptable framework for stable, model-independent reconstructions of cosmological functions and their derivatives, making it well suited to the precision era of upcoming large-scale surveys.

Acknowledgments

MP acknowledges support from the INFN project “InDark”. MP also acknowledges the participation in the COST Action CA21136 “Addressing observational tensions in cosmology with systematics and fundamental physics” (CosmoVerse). MM acknowledges funding by the Agenzia Spaziale Italiana (ASI) under agreement n. 2024-10-HH.0 and support

from INFN/Euclid Sezione di Roma. SN acknowledges support from the research project PID2024-159420NB-C43 and the Spanish Research Agency (Agencia Estatal de Investigación) through the Grant IFT Centro de Excelencia Severo Ochoa No CEX2020-001007-S, funded by MCIN/AEI/10.13039/501100011033. MP also thanks A. Favale and F. De Luca for the useful discussions.

References

- [1] P.J.E. Peebles and B. Ratra, *The Cosmological Constant and Dark Energy*, *Rev. Mod. Phys.* **75** (2003) 559 [[astro-ph/0207347](#)].
- [2] L. Perivolaropoulos and F. Skara, *Challenges for Λ CDM: An update*, *New Astron. Rev.* **95** (2022) 101659 [[2105.05208](#)].
- [3] CosmoVERSE NETWORK collaboration, *The CosmoVerse White Paper: Addressing observational tensions in cosmology with systematics and fundamental physics*, *Phys. Dark Univ.* **49** (2025) 101965 [[2504.01669](#)].
- [4] N. Schöneberg, G.F. Abellán, A.P. Sánchez, S.J. Witte, V. Poulin and J. Lesgourges, *The H_0 Olympics: A fair ranking of proposed models*, *Phys. Rep.* **984** (2022) 1 [[2107.10291](#)].
- [5] M. Seikel, C. Clarkson and M. Smith, *Reconstruction of dark energy and expansion dynamics using gaussian processes*, *Journal of Cosmology and Astroparticle Physics* **2012** (2012) 036–036.
- [6] M. Seikel and C. Clarkson, *Optimising Gaussian processes for reconstructing dark energy dynamics from supernovae*, [1311.6678](#).
- [7] A. Favale, M.G. Dainotti, A. Gómez-Valent and M. Migliaccio, *Towards a new model-independent calibration of Gamma-Ray Bursts*, *Journal of High Energy Astrophysics* **44** (2024) 323 [[2402.13115](#)].
- [8] L. Perenon, M. Martinelli, R. Maartens, S. Camera and C. Clarkson, *Measuring dark energy with expansion and growth*, *Physics of the Dark Universe* **37** (2022) 101119.
- [9] C. Bogdanos and S. Nesseris, *Genetic algorithms and supernovae type ia analysis*, *Journal of Cosmology and Astroparticle Physics* **2009** (2009) 006–006.
- [10] S. Nesseris and J. García-Bellido, *A new perspective on dark energy modeling via genetic algorithms*, *Journal of Cosmology and Astroparticle Physics* **2012** (2012) 033–033.
- [11] S. Nesseris, D. Sapone, M. Martinelli, D. Camarena, V. Marra, Z. Sakr et al., *Euclid: Forecast constraints on consistency tests of the Λ CDM model*, *Astronomy & Astrophysics* **660** (2022) A67 [[2110.11421](#)].
- [12] R. Arjona and S. Nesseris, *Novel null tests for the spatial curvature and homogeneity of the universe and their machine learning reconstructions*, *Phys. Rev. D* **103** (2021) 103539.
- [13] S. Nesseris and A. Shafieloo, *A model independent null test on the cosmological constant*, *Mon. Not. Roy. Astron. Soc.* **408** (2010) 1879 [[1004.0960](#)].
- [14] A. Aizpuru, R. Arjona and S. Nesseris, *Machine learning improved fits of the sound horizon at the baryon drag epoch*, *Phys. Rev. D* **104** (2021) 043521 [[2106.00428](#)].
- [15] J.B. Orjuela-Quintana, S. Nesseris and W. Cardona, *Using machine learning to compress the matter transfer function $T(k)$* , *Phys. Rev. D* **107** (2023) 083520 [[2211.06393](#)].
- [16] J.B. Orjuela-Quintana, S. Nesseris and D. Sapone, *Machine learning unveils the linear matter power spectrum of modified gravity*, *Phys. Rev. D* **109** (2024) 063511 [[2307.03643](#)].
- [17] J.B. Orjuela-Quintana, D. Sapone and S. Nesseris, *Fully Interpretable Emulator for the Linear Matter Power Spectrum from Physics-Informed Machine Learning*, [2407.16640](#).

[18] D.J. Bartlett, L. Kammerer, G. Kronberger, H. Desmond, P.G. Ferreira, B.D. Wandelt et al., *A precise symbolic emulator of the linear matter power spectrum*, *Astronomy & Astrophysics* **686** (2024) A209.

[19] Y. Akrami, P. Scott, J. Edsjo, J. Conrad and L. Bergstrom, *A Profile Likelihood Analysis of the Constrained MSSM with Genetic Algorithms*, *JHEP* **04** (2010) 057 [[0910.3950](#)].

[20] R. Arjona, S. Nesseris and S. Kuroyanagi, *Comparative analysis of the NANOgrav Hellings-Downs as a window into new physics*, [2412.12975](#).

[21] R. Arjona and S. Nesseris, *Reconstruction of the swampland conjectures with DESI DR1 BAO data*, *Phys. Rev. D* **112** (2025) 063504 [[2409.14990](#)].

[22] R. Arjona and S. Nesseris, *Hints of dark energy anisotropic stress using Machine Learning*, *JCAP* **11** (2020) 042 [[2001.11420](#)].

[23] M.R. Gangopadhyay, M. Sami and M.K. Sharma, *Phantom dark energy as a natural selection of evolutionary processes a la genetic algorithm and cosmological tensions*, *Phys. Rev. D* **108** (2023) 103526 [[2303.07301](#)].

[24] G. Acampora, A. Chiatto and A. Vitiello, *Genetic algorithms as classical optimizer for the Quantum Approximate Optimization Algorithm*, *Appl. Soft Comput.* **142** (2023) 110296.

[25] R. Arjona and S. Nesseris, *Hints of dark energy anisotropic stress using machine learning*, *Journal of Cosmology and Astroparticle Physics* **2020** (2020) 042–042.

[26] S. Nesseris and L. Perivolaropoulos, *Crossing the phantom divide: theoretical implications and observational status*, *Journal of Cosmology and Astroparticle Physics* **2007** (2007) 018–018.

[27] S. Nesseris and L. Perivolaropoulos, *Comparison of the legacy and gold type ia supernovae dataset constraints on dark energy models*, *Physical Review D* **72** (2005) .

[28] S. Nesseris and L. Perivolaropoulos, *Comparison of cosmological models using recent supernova data*, *Physical Review D* **70** (2004) .

[29] W.H. Press, B.P. Flannery and S.A. Teukolsky, *Numerical recipes. The art of scientific computing* (1986).

[30] J. Beyhum, E. Lapenta and P. Lavergne, *One-step smoothing splines instrumental regression*, *arXiv e-prints* (2023) arXiv:2307.14867 [[2307.14867](#)].

[31] P.C. Hansen, *The l-curve and its use in the numerical treatment of inverse problems*, vol. 4, pp. 119–142 (2001).

[32] D. Calvetti, L. Reichel and A. Shuibi, *L-curve and curvature bounds for tikhonov regularization: Theory and practice in optimization. guest editors: José mario martínez and jin yun yuan*, *Numerical Algorithms* **35** (2004) .

[33] K.P. Burnham and D.R. Anderson, *Model selection and multimodel inference: a practical information-theoretic approach*, Springer Science & Business Media (2002).

[34] D. Huterer and D.L. Shafer, *Dark energy two decades after: observables, probes, consistency tests*, *Reports on Progress in Physics* **81** (2017) 016901.

[35] E.J. Copeland, M. Sami and S. Tsujikawa, *Dynamics of dark energy*, *International Journal of Modern Physics D* **15** (2006) 1753–1935.

[36] B. Wang, E. Abdalla, F. Atrio-Barandela and D. Pavón, *Dark matter and dark energy interactions: theoretical challenges, cosmological implications and observational signatures*, *Reports on Progress in Physics* **79** (2016) 096901.

[37] V. Sahni, A. Shafieloo and A.A. Starobinsky, *Two new diagnostics of dark energy*, *Phys. Rev. D* **78** (2008) 103502.

- [38] N. Aghanim, Y. Akrami, M. Ashdown, J. Aumont, C. Baccigalupi, M. Ballardini et al., *Planck 2018 results: Vi. cosmological parameters*, *Astronomy & Astrophysics* **641** (2020) A6.
- [39] A. Adame, J. Aguilar, S. Ahlen, S. Alam, D. Alexander, M. Alvarez et al., *Desi 2024 vi: cosmological constraints from the measurements of baryon acoustic oscillations*, *Journal of Cosmology and Astroparticle Physics* **2025** (2025) 021.
- [40] A. Favale, A. Gómez-Valent and M. Migliaccio, *Cosmic chronometers to calibrate the ladders and measure the curvature of the Universe. A model-independent study*, *Mon. Not. Roy. Astron. Soc.* **523** (2023) 3406 [[2301.09591](#)].
- [41] E. Tomasetti, M. Moresco, N. Borghi, K. Jiao, A. Cimatti, L. Pozzetti et al., *A new measurement of the expansion history of the universe at $z = 1.26$ with cosmic chronometers in vandels*, *Astronomy & Astrophysics* **679** (2023) A96.
- [42] R. Jimenez and A. Loeb, *Constraining cosmological parameters based on relative galaxy ages*, *Astrophys. J.* **573** (2002) 37 [[astro-ph/0106145](#)].
- [43] M. Moresco, R. Jimenez, L. Verde, A. Cimatti and L. Pozzetti, *Setting the stage for cosmic chronometers. ii. impact of stellar population synthesis models systematics and full covariance matrix*, *The Astrophysical Journal* **898** (2020) 82.
- [44] Euclid Collaboration, A. Blanchard, S. Camera, C. Carbone, V.F. Cardone, S. Casas et al., *Euclid preparation. VII. Forecast validation for Euclid cosmological probes*, *Astronomy & Astrophysics* **642** (2020) A191 [[1910.09273](#)].
- [45] DESI Collaboration, A. Aghamousa, J. Aguilar, S. Ahlen, S. Alam, L.E. Allen et al., *The DESI Experiment Part I: Science, Targeting, and Survey Design*, *arXiv e-prints* (2016) [arXiv:1611.00036](#) [[1611.00036](#)].

A Testing Λ CDM with a subset of current data

In the main analysis (Section 3.2.1), we adopted a conservative approach by utilising the full available dataset of CC up to $z \approx 2$, regardless of the precision of individual measurements. However, the CC dataset is heterogeneous, combining measurements from various surveys with different sensitivities and systematics. As GA is driven by the optimisation of the χ^2 statistic, data points with large uncertainties contribute less to the fitness of the solution but can still introduce stochastic noise, particularly in the reconstruction of the derivative $H'(z)$. To verify the impact of these lower-precision measurements on our results, we performed an additional run of the **GAME** pipeline using a quality-cut subset of the data. In this subsample, we excluded data points with value $H > H_{\text{mean}} + 2\sigma_H$. This threshold removes the measurements with the lowest constraining power, which are often those most susceptible to large systematic effects or low signal-to-noise ratios.

A.1 Impact on the reconstruction of $H(z)$

The reconstruction of $H(z)$ and its derivative using this high-quality subset generates results that are fully consistent with the full-dataset analysis but differ enhancing more stability. While the reconstruction of $H(z)$ remains largely unchanged, confirming the robustness of **GAME** averaged reconstructions, the improvement is most notable in the derivative $H'(z)$. In the full analysis (Figure 7), the derivative exhibits fluctuations at high redshifts ($z > 1.2$) where the data is sparser and noisier. By removing the points with large error bars, the resulting $H'(z)$ becomes significantly smoother and tracks Λ CDM prediction more closely. This suggests that the slight oscillatory features observed in the main analysis are likely

artifacts driven by the scatter of low-precision data points rather than physical deviations from the standard model. Furthermore, the exclusion of these outliers decreases the path-integral uncertainty estimation δf_{PI} .

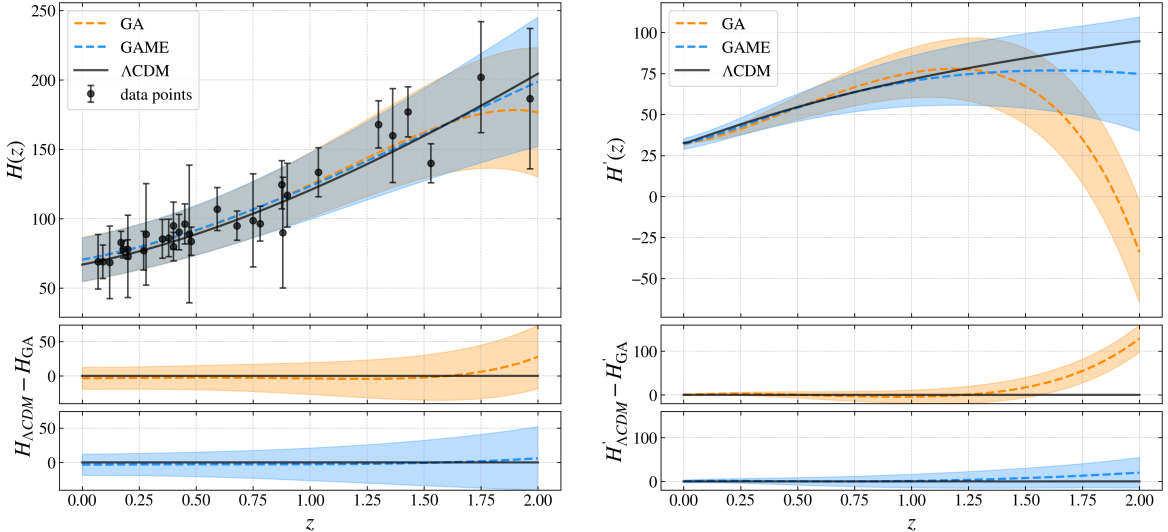


Figure 12. Comparison of the reconstructed $H(z)$ and $H'(z)$ obtained from the quality-cut CC subset (excluding points with $H > H_{\text{mean}} + 2\sigma_H$). The plotting style matches Figure 7: the solid black curve represents ΛCDM , the orange dashed curve is the standard GA best-fit, and the blue dashed curve is the GAME averaged reconstruction. *Left:* The $H(z)$ reconstruction remains stable and in excellent agreement with the result from the full dataset, demonstrating that the GAME approach is robust to the exclusion of low-quality measurements. *Right:* The $H'(z)$ reconstruction becomes noticeably smoother relative to the full-sample case. Eliminating the high-uncertainty outliers mitigates the large fluctuations at high redshift seen in the main analysis, generating a derivative profile closer to the ΛCDM prediction and a lower path-integral uncertainty.

A.2 Impact on the derivation of $w(z)$

The smoothness of $H'(z)$ has a direct consequence on the derivation of the dark energy equation of state $w(z)$. Since $w(z)$ depends on the ratio of terms involving both $H(z)$ and $H'(z)$, any unphysical fluctuation in the derivative is amplified in the equation of state. Using the subset, we observe that the divergence of the confidence intervals for $w(z)$ at $z > 1.5$ is slightly mitigated, although the mathematical singularity inherent to the vanishing dark energy density $\Omega_{\text{de}} \rightarrow 0$ remains the dominant factor. More importantly, the constraints at low redshift ($z < 1$) remain tight and centered on $w = -1$. When adopting the DESI prior for $\Omega_{m,0}$, we find a stronger constraint than that derived using the full sample without excluding the noisiest measurements (Equation (3.3)):

$$w(0) = -0.988 \pm 0.101, \quad (\text{A.1})$$

reinforcing the conclusion that the local universe is consistent with a cosmological constant. This test demonstrates that while the inclusion of all available data is statistically complete, the future of model-independent reconstructions lies in the acquisition of high-precision CC measurements rather than simply increasing the data sample.

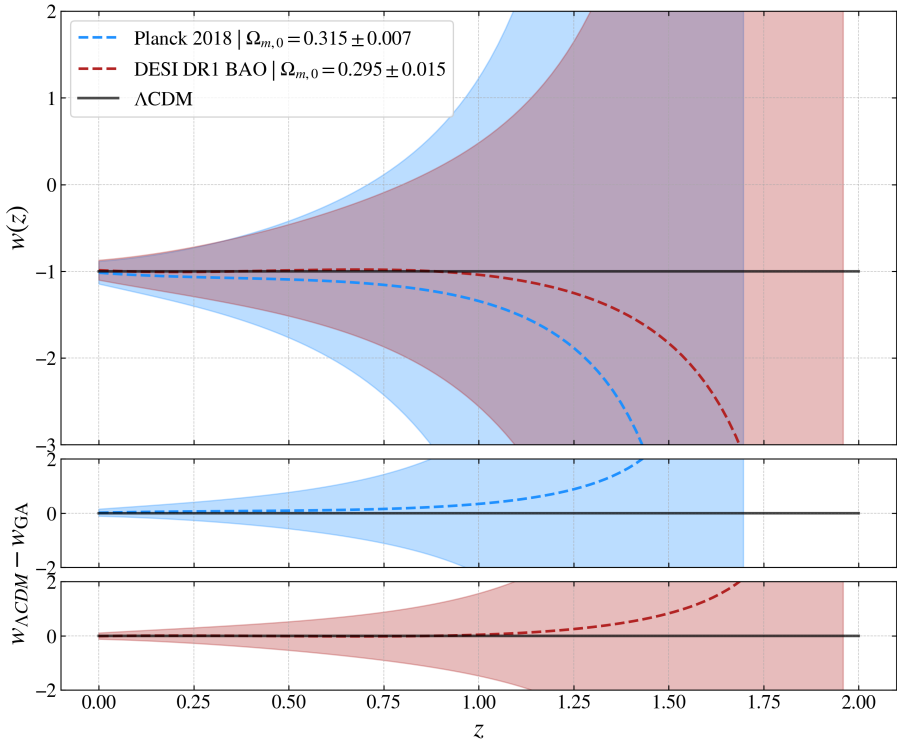


Figure 13. Reconstruction of the dark energy equation of state $w(z)$ obtained from the quality-cut CC subset. As in Figure 8, the blue dashed curve corresponds to imposing the Planck 2018 prior on $\Omega_{m,0}$, while the red dashed curve adopts the DESI DR1 BAO prior. Removing the noisiest measurements leads to a slightly more stable behavior at intermediate redshifts, while retaining the tight constraints at $z < 1$, which continue to be centered on the cosmological constant value $w = -1$ (solid black line). At high redshift ($z > 1.5$), the confidence regions still broaden because the dark energy density tends to zero ($\Omega_{de} \rightarrow 0$), reinforcing that the weakening of constraints in this regime is inherent to the chosen parametrisation rather than driven by low-quality data.

B Hyperparameter configurations setup

Table 1 summarises the GA hyperparameters used for the two reconstructions discussed in this work: the validation test function $f(x)$ (Section 2.3.3) and the CC reconstruction of the Hubble rate $H(z)$ (Section 3.2.1 and Section 3.3.1). For each target quantity we run the GA over an ensemble of N_{conf} configurations, which differ by the adopted grammar choice and by stochastic realisations (random seeds). The GA population size (N_{pop}), the maximum number of generations (N_{gen}), and the genetic operators rates (selection, crossover, mutation) are fixed within each reconstruction setup.

Hyperparameter	$f(x)$	$H(z)$
Maximum generations N_{gen}	3000	3000
Population size N_{pop}	100	100
Grammar set	[poly] [cpl] [poly, cpl]	[poly, cpl, exp] + perm. [poly, exp] + perm. [poly], [exp], [cpl]
Selection rate	0.30	0.30
Crossover rate	0.85	0.85
Mutation rate	0.85	0.85
Number of random seeds N_{seeds}	33	10
Number of configurations N_{conf}	99	150

Table 1. Hyperparameter setup adopted for the GA reconstructions. Here “perm.” indicates that all orderings (permutations) of the listed building blocks are included.